Manufacturing Letters 29 (2021) 1–4

Contents lists available at ScienceDirect

Manufacturing Letters

journal homepage: www.elsevier.com/locate/mfglet

Letters

Effect of spiral scan strategy on microstructure for additively manufactured stainless steel 17–4

H. Yeung [a,*], J. Chen [b], G. Yang [c], Y. Guo [b], D. Lin [c], W. Tan [d], J. Weaver [a]

[a] National Institute of Standards and Technology, Gaithersburg, MD 20899, United States
[b] Department of Mechanical Engineering, Michigan State University, East Lansing, MI 48824, United States
[c] Department of Industrial and Manufacturing Systems Engineering, Kansas State University, Manhattan, KS 66506, United States
[d] Department of Mechanical Engineering, University of Utah, Salt Lake City, UT 84112, United States

ARTICLE INFO

Article history:
Received 29 January 2021
Received in revised form 16 April 2021
Accepted 26 April 2021
Available online 30 April 2021

Keywords:
Additive manufacturing
Scan strategies
Microstructure
Hardness

ABSTRACT

The effect of the scan strategy on microstructure is investigated using a custom-built laser powder bed fusion additive manufacturing testbed. Eight stainless steel cubic parts were built to compare two different scan strategies: raster and spiral. The processes were monitored in-situ by a high-speed camera coaxially aligned to the heating laser, and the parts built were characterized by micro-indentation and optical microscopy. The spiral scan strategy creates a much larger meltpool area and the resulting parts exhibit an equiaxed grain structure with 54% higher hardness value compared to the raster scan strategy.

1. Overview

Laser powder bed fusion (LPBF) uses a high-power laser to melt and solidify thin layers of metal powder into geometric patterns sliced from parts' solid models [1]. A typical LPBF process scans the laser back and forth with constant power and speed, and along straight hatching lines to cover the build area. Most reported studies on the effects of scan strategy on microstructure and properties were done by simply changing the orientation and length of the hatching lines, or the island (strip) size, to change the thermal history [2–4]. The variations in the solidified microstructure [5,6] mainly come from the meltpool morphology variation due to dynamic thermal history [7]. Platt et al. improved the hardness of additively manufactured stainless steel 17–4 parts by 36% by scanning the layer twice and adding an idle time by 'virtual parts' [8]. Kürnsteiner et al. fabricated Damascus steel in a directed energy deposition process by pausing the process for 120 s for every four layers [9]. These studies demonstrated the potential of utilizing intrinsic heat treatment during the additive manufacturing (AM) process to achieve microstructure control. In this study, we propose a new spiral scan strategy, which covers the build area using a continuous circular spiral scan path instead of a discontinued hatching line path. The repeated circular pattern created a more homogenous reheating effect, which is controllable by adjusting the spiral size. It was shown the spiral scan significantly increased the hardness of 17–4 stainless steel parts compared to the raster scan strategy. This is likely due to the equiaxed grain size achieved by the spiral scan. Therefore, the spiral scan is believed to be superior for microstructure control in comparison to raster scan strategies. The spiral strategy is not available on commercial machines. An in-house developed open-platform testbed is used to build the parts in this study.

2. Open platform AM process control and scan strategies

AM process preparation contains three major steps: (1) Digitally slice parts' solid models into layers. (2) Assign scan path/vectors for each layer. (3) Interpolate scan vectors into time-stepped point commands. Fig. 1 shows the format of the point commands created by the in-house developed Simple Additive Manufacturing (SAM) software [10]. The point commands are an $n \times m$ numerical array, where n is the number of time steps in 10 µs increments, and m is the number of control parameters. This format is based on the xy2-100 protocol for the laser-galvo position (X, Y), but has been extended to include the control of laser power (L), laser spot size (D), and triggers (T) for synchronizing process monitoring sensors, such as a coaxial meltpool monitoring camera shown in Fig. 1. The coaxial camera captures meltpool incandescent emission diverted by a dichroic mirror and filtered at the emission bandwidth of

* Corresponding author.
E-mail address: ho.yeung@nist.gov (H. Yeung).

https://doi.org/10.1016/j.mfglet.2021.04.005
2213-8463/Published by Elsevier Ltd on behalf of Society of Manufacturing Engineers (SME).

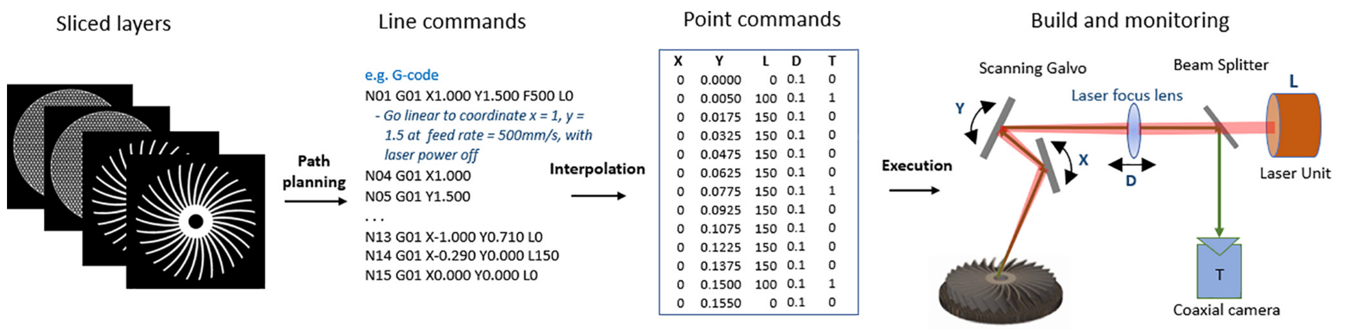

Fig. 1. Open platform AM process control. The part's solid model is sliced into layers, each layer is covered with scan lines, each line is interpreted into points, and then sent to AM controller for execution.

(850 ± 20) nm. The point commands allow full user control of the process dynamics and fully synchronized in-situ monitoring. The use of time-stepped point commands is a truly open platform approach and provides a full description of the scan strategy and the geometry of a part. Most importantly, it enables the implementation of novel scan strategies such as in [11–13]. In this study, we report a new spiral scan strategy implemented with the point commands and compare its effect on hardness and microstructure with the raster scan strategies.

3. Experiments and meltpool monitoring

Eight 17–4 stainless steel rectangular parts of 10 mm in length, 5 mm in width, and 10 mm in height (build direction) were built with EOS GP1[1] powder [14] using two scan strategies: raster and spiral. Islands of different sizes were used, with details in Fig. 2(a). Raster 2x4, for example, means raster scan strategy with 8 islands by dividing the scan area into 2 parts along the width and 4 parts along the length. Scan paths for parts #2 and #8, representing the typical spiral and raster scan strategies, are shown in Fig. 2(b). The spiral scan strategy covers the build area by a continuous circular path, and there is no interruption for laser power for the whole length. The raster scan strategy uses straight lines; laser power is switched off at end of each line. This strategy is also known as 'skywrite'. In all cases the nominal laser power is 285 W, laser speed is 960 mm/s, hatching spacing is 0.1 mm, laser spot size is 85 μm, layer thickness is 40 μm, and interlayer rotation angle is 90 degrees counter-clockwise (for raster scans only). The parts were built in an argon environment with a laminar flow of 300 L/min. The process was monitored in-situ by a coaxial camera (Fig. 1); the meltpool images were captured at 20 K frames/s. The meltpool area average and standard deviation (std) for each part are shown in Fig. 2(c). The average meltpool area of spiral scans (part #1 to #3) depends on the spiral size, and it is much larger than the raster scans (part #4 to #8). The island size has very little effect on the meltpool area for raster scans.

4. Mechanical properties

Micro Vickers hardness tests were used to probe the mechanical properties of the as-fabricated parts. The tests were performed on the surface normal to the build direction (build plane). The surface was polished before the test with the final polishing using colloidal alumina of 0.3 μm particle size. For all tests, a 200 g force and a 10 s dwell time were used. At least 10 indents were conducted on each part. Fig. 3 shows the measured hardness results. Parts fabricated by raster scans (#4 to #8) have essentially the same average hardness value of about 225 HV, irrespective of the island size. This agrees with the manufacturer's specification for the as-built hardness of 230 ± 20 HV for EOS GP1 powder [14]. In contrast, parts fabricated by spiral scans with smaller spiral sizes (#2 and #3) have a significantly higher average hardness value of about 350 HV, which represents a 54% increase in hardness from parts fabricated by raster scans. In fact, the hardness achieved by spiral scan has exceeded most previously reported hardness values for as-fabricated 17–4 [8,15] and is similar to those fabricated by "double" scan strategies in [15] but with more uniform hardness distributions indicated by smaller std. Results show that the hardness from spiral scan depends on the spiral size. Part #1, fabricated with a larger spiral size, has an average hardness of 255 HV. Though this value is higher than those for raster scans, it is much lower than those for parts #2 and #3, which have smaller spiral sizes. Therefore, the spiral size is a critical parameter of the spiral scan strategy in controlling the properties of fabricated parts.

5. Microstructures

All parts were ground and polished to a mirror finish using a final diamond suspension of 0.1 μm. The polished parts were then cleaned with 100% ethanol. The cleaned parts were electro-etched in a solution of 60% nitric acid. During the electro-etching, the initial voltage was set to 2 V and carefully increased until the current reached around 100 mA. After 15 s to 30 s of etching, the parts were cleaned with water and observed under an optical microscope. Fig. 4 shows the microstructure of stainless steel 17–4 for the build plane (same plane that was indented) for part #2 (spiral) and #6 (raster). The spiral scan generates a large molten pool. The overall temperature gradient for the molten pool solidification should be along the build direction, which drives the microstructure to grow along the build direction. On a horizontal plane (build plane) as shown in Fig. 4(a), the morphology is found to be equiaxed dendritic, but the equiaxed cells are likely the cross-sections of the vertically growing columnar dendrites. On the other hand, the raster scan for part #6 generates a thermal history, with the direction of temperature gradient for molten pool solidification varying for different passes and layers. As a result, the microstructure in Fig. 4(b) is cellular along with different directions, according to the direction of the temperature gradient when the local molten pool is solidified. The spiral scan for part #2 possibly generates a lower cooling rate for the molten pool and the entire part. This may explain the relatively large microstructure dimension in Fig. 4(a), but also indicate the hardness improvement is not because the grain size refinement. One possible reason could be

[1] Certain commercial equipment, instruments, or materials are identified in this paper in order to specify the experimental procedure adequately. Such identification is not intended to imply recommendation or endorsement by NIST, nor is it intended to imply that the materials or equipment identified are necessarily the best available for the purpose.

#1. Spiral 2x1, 161s	#2. Spiral 4x1, 191s	#3. Spiral 8x1, 209s	#4. Raster 1x2, 128s
#5. Raster 1x4, 162s	#6. Raster 1x1, 110s	#7. Raster2x1, 142s	#8. Raster 2x4, 198s

(a)

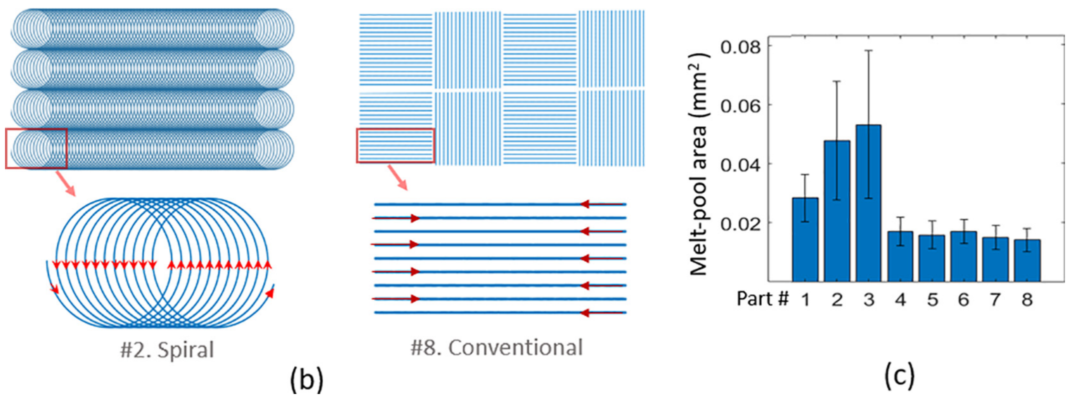

Fig. 2. (a) Scan strategies and build time for part #1 to #8. Build time is calculated based on the total galvo scan time. (b) Scan paths for parts #2 (left) and #8 (right), representing the typical spiral and raster scans. The lower is the enlarged views of the regions in the red boxes. The arrows indicate the scan directions. (c) Average meltpool area with ± 1 std for part #1 to #8. (For interpretation of the references to colour in this figure legend, the reader is referred to the web version of this article.)

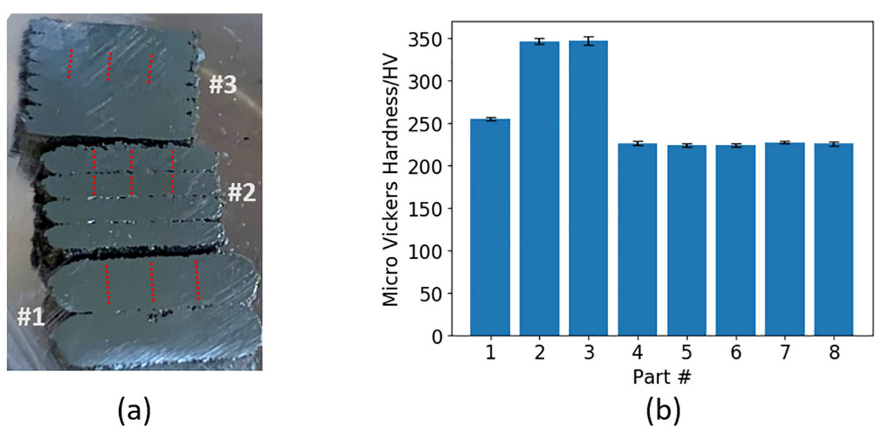

Part	#1	#2	#3	#4	#5	#6	#7	#8
Average (HV)	255	346	347	226	224	224	227	226
1-Std (HV)	2	4	5	2	2	2	2	3

(c)

Fig. 3. Hardness measurement. (a) Positions (marked by red dots) at which hardness measurements were taken. (b) Bar chart shows average hardness with ± 1 std. (c) Table shows the average hardness. (For interpretation of the references to colour in this figure legend, the reader is referred to the web version of this article.)

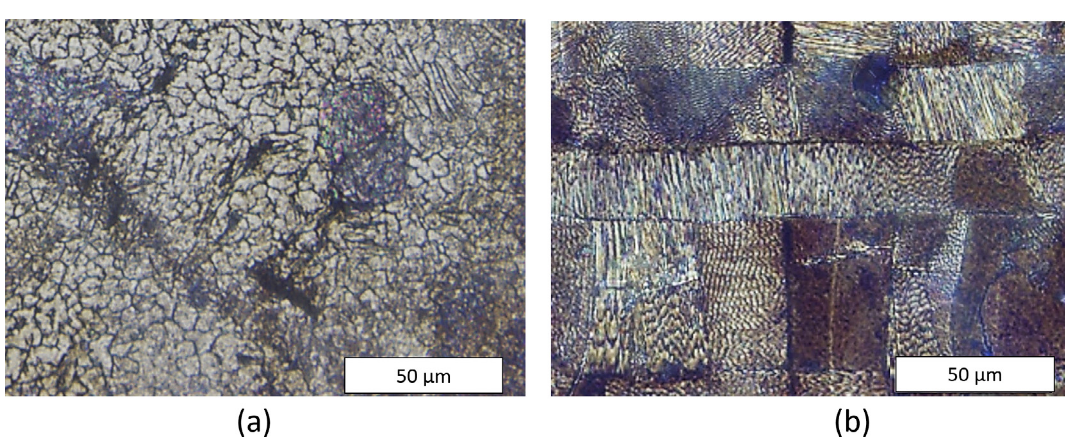

Fig. 4. Microscopic images for (a) part #2 (spiral scan), and (b) part #6 (raster scan).

the phase change in 17–4 during the re-heating and cooling process created by the spiral scan. Further studies are needed to identify the correlation between the microstructure and hardness in these parts.

6. Summary and future work

A spiral scan strategy is developed, which results in a constant larger meltpool determined from in-situ monitoring comparing to raster scan strategies at the same laser power level. The parts built with the spiral scan strategy shows a 54% increase in hardness and a distinct microstructure. It is speculated the larger meltpool and the reheating by the spiral scan strategy significantly changed the solidification process. Electron backscatter diffraction (EBSD) is planned to further quantify the grain and crystal structure as well as to study the possible phase changes.

Declaration of Competing Interest

The authors declare that they have no known competing financial interests or personal relationships that could have appeared to influence the work reported in this paper.

References

[1] Yap CY, Chua CK, Dong ZL, Liu ZH, Zhang DQ, Loh LE, et al. Review of selective laser melting: materials and applications. Appl Phys Rev 2015;2(4):041101. https://doi.org/10.1063/1.4935926.
[2] Thijs L, Verhaeghe F, Craeghs T, Humbeeck JV, Kruth J-P. A study of the microstructural evolution during selective laser melting of Ti–6Al–4V. Acta Mater 2010;58(9):3303–12. https://doi.org/10.1016/j.actamat.2010.02.004.
[3] Lu Y, Wu S, Gan Y, Huang T, Yang C, Junjie L, et al. Study on the microstructure, mechanical property and residual stress of SLM Inconel-718 alloy manufactured by differing island scanning strategy. Opt Laser Technol 2015;75:197–206. https://doi.org/10.1016/j.optlastec.2015.07.009.
[4] Rafi HK, Pal D, Patil N, Starr TL, Stucker BE. Microstructure and mechanical behavior of 17–4 precipitation hardenable steel processed by selective laser melting. J Mater Eng Perform 2014;23(12):4421–8. https://doi.org/10.1007/s11665-014-1226-y.
[5] Criales LE, Arısoy YM, Lane B, Moylan S, Donmez A, Özel T. Laser powder bed fusion of nickel alloy 625: experimental investigations of effects of process parameters on melt pool size and shape with spatter analysis. Int J Mach Tools Manuf 2017;121:22–36. https://doi.org/10.1016/j.ijmachtools.2017.03.004.
[6] Stoudt M, Williams ME, Levine LE, Creuziger AA, Young SW, Heigel JC, et al. Location-specific microstructure characterization within In625 additive manufacturing benchmark test artifacts. Integrating Mater Manuf Innov 2020; Special Issue of the AM-Bench 2018 Test Series.
[7] Heigel J, Lane B, Phan T, Brown D, Strantza M, Levine L. Sample design and in-situ characterization of cooling rate and melt pool length during 3D AM builds of 15–5 and IN625 AM-Bench artifacts. Integrating Mater Manuf Innov 2019.
[8] Platt S, Wegner J, Kleszczynski S, Witt G. Effect of scan strategy, re-melting and exposure time on the microstructure of stainless steel 17 - 4 PH fabricated by laser powder bed fusion of metals. 7th Int Conf Addit Technol ICAT 2018 At Maribor Slov n.d.
[9] Kürnsteiner P, Wilms MB, Weisheit A, Gault B, Jägle EA, Raabe D. High-strength damascus steel by additive manufacturing. Nature 2020;582(7813):515–9. https://doi.org/10.1038/s41586-020-2409-3.
[10] Yeung H, Lane BM, Donmez MA, Fox JC, Neira J. Implementation of Advanced Laser Control Strategies for Powder Bed Fusion Systems. 46th SME North Am Manuf Res Conf NAMRC 46 Tex USA 2018; 26:871–9. https://doi.org/10.1016/j.promfg.2018.07.112.
[11] Yeung H, Lane B, Fox J. Part geometry and conduction-based laser power control for powder bed fusion additive manufacturing. Addit Manuf 2019;30:100844. https://doi.org/10.1016/j.addma.2019.100844.
[12] Yeung H, Lane B. A residual heat compensation based scan strategy for powder bed fusion additive manufacturing. Manuf Lett 2020;25:56–9. https://doi.org/10.1016/j.mfglet.2020.07.005.
[13] Yeung H, Yang Z, Yan L. A meltpool prediction based scan strategy for powder bed fusion additive manufacturing. Addit Manuf 2020;35:101383. https://doi.org/10.1016/j.addma.2020.101383.
[14] EOS StainlessSteel GP1 n.d. https://www.eos.info/en/additive-manufacturing/3d-printing-metal/dmls-metal-materials/stainless-steel.
[15] Rashid R, Masood SH, Ruan D, Palanisamy S, Rahman Rashid RA, Brandt M. Effect of scan strategy on density and metallurgical properties of 17–4PH parts printed by selective laser melting (SLM). J Mater Process Technol 2017;249:502–11. https://doi.org/10.1016/j.jmatprotec.2017.06.023.